Title:	**Advanced Structural Silicone Glazing**
Authors:	Jon Kimberlain, Application Specialist, Dow Corning Corporation Lawrence Carbary, Senior Member, Dow Corning Corporation Charles D. Clift, Senior Principal, Curtain Wall Design and Consulting, Inc. Peter Hutley, Engineer, Curtain Wall Design and Consulting, Inc.
Subjects:	Building Materials/Products Façade Design
Keywords:	Façade Structure
Publication Date:	2012
Original Publication:	CTBUH 2012 9th World Congress, Shanghai
Paper Type:	1. Book chapter/Part chapter 2. Journal paper 3. **Conference proceeding** 4. Unpublished conference paper 5. Magazine article 6. Unpublished

Advanced Structural Silicone Glazing

先进的结构性有机硅玻璃

Jon Kimberlain

Larry Carbary

Charles D. Clift

Peter Hutley

Jon Kimberlain & Larry Carbary

Dow Corning Corporation
760 Hodgenville Road
Elizabethtown, Kentucky
USA 42701

tel (电话): +1 270.706.8301
fax (传真): +1 270.706.8340
email (电子邮箱): jon.kimberlain@dowcorning.com, l.carbary@dowcorning.com
www.dowcorning.com

Jon Kimberlain is an Application Specialist with Dow Corning Corporation and has been involved in the production, commercialization and application of weatherproofing and structural glazing sealants.

Jon Kimberlain为道康宁公司应用技术专家，从事硅酮耐候密封胶和硅酮结构密封胶的生产、商业化与应用。

Larry Carbary is the senior member of Dow Corning's Construction Technical Service Staff working on new technologies for commercial façades.

Larry Carbary现为道康宁建筑工业技术服务团队的资深成员，也是幕墙新技术研发方面的科学家。

Charles D. Clift & Peter Hutley

Curtain Wall Design and Consulting, Inc
8070 Park Lane Suite 400
Dallas, Texas
USA 75231

tel (电话): +1 972.437.4200
email (电子邮箱): cclift@cdc-usa.com, phutley@cdc-usa.com
www.cdc-usa.com

Mr. Charles Clift is Senior Principal and President of Curtain Wall Design and Consulting, Inc. (CDC). He has worked at CDC in Dallas, Texas for 30 years providing engineering design for curtain walls and other exterior cladding systems.

Clift先生是幕墙设计与咨询公司（CDC）的高级负责人与总裁。他在位于德克萨斯州达拉斯市的CDC效力已经30年，主要致力于幕墙及其他外部覆层系统的工程设计工作。

Peter Hutley is a graduate engineer at Curtain Wall Design & Consulting. Since graduating from Rice University in 2010, Mr. Hutley has been responsible for the structural and thermal engineering of façade systems.

Peter Hutley是一位幕墙设计与咨询见习工程师。自2010年从莱斯大学毕业以来，他一直负责幕墙系统的结构与热工程。

Abstract

This paper presents an advanced engineering evaluation to improve structural silicone glazing (SSG) design in high-performance curtain wall systems. High wind pressures often result in bulky SSG profile dimensions. Architectural desire for slender curtain wall sight-lines and reduction in aluminum usage led to optimization of structural bite geometry for improved stress distribution through use of finite element analysis of the hyperelastic silicone. This advanced design technique compared to traditional SSG design highlights differences in stress distribution contours in the silicone material. Full scale specimens were performed to verify design capacity in addition to correlation of physical test results with theoretical simulation to provide confidence of the model. This design technique will introduce significant engineering advancement to the curtain wall industry.

Keywords: Structural Silicone Glazing, Finite Element Analysis, Hyperelastic Modeling

摘要

本文提出了一种先进的工程评价方法，来改善高性能幕墙系统中的结构硅酮胶玻璃装配（SSG）设计。 高风压常常会导致庞大的SSG框架尺寸，而建筑上则希望实现苗条的幕墙视线和较少的铝材使用，因此需要通过对超弹性硅酮胶的有限元分析来改善应力分布，从而达到优化结构胶宽度的几何尺寸。与传统的结构性装配设计相比，这种先进的设计技术突出了硅酮材料中应力分布曲线的不同。为了增强对设计模型的信心，除了将物理测试结果与理论模拟关联起来之外，还足尺样本进行了性能测试。该设计技术将会对幕墙工业的工程水平带来显著的提升。

关键词：结构硅酮胶玻璃装配，有限元分析，超弹性建模

Structural Silicone Glazing Yesterday and Today

Silicone structural glazing originated in 1965 with the use of glass-to-glass structural seals in the PPG Total Vision System. The practice further developed into two-sided applications in 1970, which utilized two sides of the glass infill adhered to metal framing members using silicone sealants, typically vertical jambs, with the head and sill of the glazing captured into a glazing channel with compression glazing. Four-sided applications, where silicone sealants were solely utilized to attach glass to metal mullions, were first utilized in 1971. Use of innovative glass products yielded two-sided and four-sided applications of insulating glass units in 1976 and 1978 respectively (Hilliard et. al 1977).

Structural silicone glazing has been studied with respect to high-performance environments for the last several decades with proven durability and performance in areas of high wind zones, hurricane/typhoon prone areas, extreme temperatures, and seismic activity (Carbary 2007).

However, the basic design theory on how to properly size the structural joint has remained the same. The bite calculation as derived from the trapezoidal loading theory is as follows

结构硅酮胶玻璃的昨日与今朝

结构硅酮胶玻璃装配始于1965年PPG全玻幕墙系统中玻璃对玻璃结构密封的使用。1970年，实践进一步发展到两边结构胶应用，采用的是用硅酮密封胶将玻璃的两边粘接在金属框架构件上，典型的玻璃装配是在垂直侧柱打胶，玻璃的顶部和底部以压式装玻璃件固定在装玻璃槽上。自1971年开始使用四边打胶应用，即单独使用硅酮密封胶来连接玻璃与金属竖框。开始使用创新的玻璃产品后，在1976年和1978年分别实现了中空玻璃单元的两边和四边打胶应用（Hilliard等，1977）。

过去的几十年中，在高性能环境下对结构硅酮胶玻璃装配进行了研究，证明其在强风区域、易发生飓风/台风的区域、极端温度区域和地震活动区域均具有良好的耐久性和表现（Carbary，2007）。

但是，关于如何确定结构胶宽度尺寸的基本设计理论仍不改变。由梯形应力分布理论得出的结构胶宽度计算如下：

$$\text{结构胶宽度} = \frac{0.5 \times \text{短边长度} \times \text{风荷载}}{\text{密封胶设计强度}}$$

出版于1989年的ASTM文章“结构硅酮密封胶连接尺寸的计算方法”讨论了矩形玻璃装配单元的结构连接宽度是基于玻璃尺寸、梯形应力分布原则、最大风荷载和最大为20 psi的密封胶设计强度的简单物理

$$\text{Bite} = \frac{0.5 \times \text{short span length} \times \text{wind load}}{\text{Sealant design strength}}$$

The ASTM article, "Methods for Calculating Structural Silicone Sealant Joint Dimensions," published in 1989,discussed the structural joint width for a rectangular glazing unit is based on the simple physical relationship of the size of the glass, trapezoidal loading principle, maximum windload, and a maximum sealant design strength of 20 psi (Haugsby et. al 1989).

- The windload is the maximum determined force of pressure due to wind speed
- Short span is the shortest dimension of the four sides of rectangular glazing unit
- Sealant design strength is the maximum tensile force allowed on the sealant

Sealant technology, analytical techniques, and computing technology has significantly advanced over the history of the practice of structural glazing. Sealant technology has progressed with neutral curing formulations, increased tensile strengths, and higher movement capability. Studies have been conducted on the performance of sealants in specialized applications. Several papers have been written on the use of silicone sealants in curtain wall units for seismic activity (Zarghamee et al 1996) including the use of finite element analysis to predict the mode of failure in silicone joint (Broker et al 2012).

A study entitled "Evaluation of Silicone Sealants at High Movement Rates Relevant to Bomb Mitigating Window and Curtainwall Design", used high-speed photography and specialized measuring devices that illustrated the relationship of the tensile capability of the sealant increases as the speed increases to validate the successful use in ballistic applications (Yarosh et al 2008).

The basis for design strength and method of design are not addressed in these papers. For good reason, as the design has been used in projects over the world that has performed well in excess of 40 years. ASTM C1401 Standard Guide for Structural Sealant Glazing is the most complete reference to the design considerations for structural silicone glazing. This document provides an excellent overview of the practice along with a full list of historical references regarding the subject.

There have been efforts to challenge both the basis of designing structural joints and increasing design strengths as mentioned above. Unfortunately, there have been no thoroughly developed and published technical arguments for proof of challenges. Opportunistic approaches appear to be based on short-term business risks and rewards with no regard to impacts of durability based on sound science and engineering.

Finite element analysis of structural silicone has been used to explore standard (Travis et al 1998) and unique designs (Hagl 2008) coupled with the understanding of the non-linear behavior of structural silicone materials. This tool, which has been used in the aerospace and automotive industries, has expanded the understanding of non-linear materials in the construction industry.

Finite Element Modeling of SSG

Advanced computer software analysis can provide access to several hyperelastic material properties, as well as curve-fitting subroutines that can be used to automatically generate material property data from physical testing. The services of Axel Products were used to develop accurate tension, shear, and biaxial extension data for Dow Corning(R)

关系（Haugsby等，1989）。

- 由于风速风荷载是压力的最大决定力，
- 小跨度是矩形玻璃装配单元四边的最短尺寸，
- 密封胶设计强度是密封胶上允许的最大拉应力。

密封胶技术、分析技术和计算技术在结构玻璃装配实践的历史上取得了显著的进展。密封胶技术随着中性固化配方、增加拉伸强度和更高的位移能力而发展。在各种具体的应用中对密封胶的性能已进行了研究，另有几篇有关在幕墙单元中硅酮密封胶于地震活动中使用的文章（Zarghamee等，1996），包括用于预测硅酮胶接缝失效方式的有限元分析（Broker等，2012）。

一项使用高速摄影和专业测量装置的研究"在与爆炸减震窗和幕墙设计相关的高移动率下的硅酮密封胶的评价"显示了密封胶的拉伸能力随着速度而提高的关系，验证了在弹道应用中的成功使用（Yarosh等，2008）。

这些文章中没有强调设计强度与设计方法的依据。这是有原因的，设计已经在全世界的项目中使用，且在四十多年的时间里运行良好。ASTM C1401结构密封胶玻璃装配标准指南是结构硅酮玻璃装配设计考虑的最完整的参考。本文提供了良好的实践概况，以及有关这主题的一系列完整历史参考资料。

以上所提及的结构连接设计与提高设计强度的两项根据一直被受挑战。可惜，尚未有完全成熟的、公开发布的技术论据来证实这些挑战。机会主义方法似乎是基于短期的经营风险与回报的，没有顾及基于合理科学与工程的耐久性影响。

结构硅酮的有限元分析，结合了对结构硅酮材料非线性性质的理解，一并被用来探索标准（Travis等，1998）和独特的设计（Hagl，2008）。该工具一直被应用于航空和汽车工业，扩展了在建筑工业中非线性材料的理解。

结构硅酮胶玻璃装配的有限元建模

通过先进的计算机软件分析可以获取几种超弹性材料的属性，同时从物理测试中使用曲线拟合子程序来自动产生材料属性数据。Axel产品的服务已被用于开发道康宁（R）983结构性装配硅酮密封胶的准确拉伸强度、剪力与双轴伸展数据。然后用软件分析将几种材料模型的Axel拉伸强度、剪力和双轴数据的数据模型进行曲线拟合，以查找一条根据提供数据能最少化缩放残值的曲线拟合。不可压缩的二元Mooney-Rivlin曲线被选择用来进行拟合，因为其缩放残值最小。独立文献显示Mooney-Rivlin材料模型可以精确地显示一种材料对高达100%拉紧的反应。

采用1.27 mm粒度对Mooney-Rivlin二元模型进行试验，并与道康宁进行的ASTM C1135拉伸粘合连接样品试验的结果进行对比。下面记录了用于复制ASTM C1135试验样品的模型，其硅酮胶接口的尺寸为50.8 mm x 12.7 mm x 12.7 mm。为了提高计算效率，附着在硅酮胶上玻璃尺寸被减小到了硅酮胶样品本身的表面积。

将ASTM C1135试验模型的结果与Axel产品曲线拟合数据中使用的同一批硅酮胶的物理试验样本结果进行了比较。图1记录了ASTM C1135试验结果和C1135 ANSYS FEA结果的载荷与偏移图。此外，表1中提供了每1.27 mm偏移的结果，以及每个点的合力误差。

单批硅酮胶的曲线拟合方法结果显示，在3.81mm偏移范围内或约30%额定应变下记录到的最大误差为17.6%。在所有的情况下，FEA结果均超过预期的物理试验结果。该批次硅酮胶观察到的百分比误差显示：虽然材料性能比测试结果更强，但在整个模型延伸范围内试验与模型材料之间的偏差一直在11%与18%之间。应当注意，用于生成FEA材料性质的数据的应变率与用于生成ASTM C1135试验结果的数据的应变率是不同的；FEA材料性质是在0.01 s^{-1}的应变率下生成的，而ASTM C1135试验结果则是在0.0167 s^{-1}的应变率下生成的。已知超弹性材料的应变率对模量

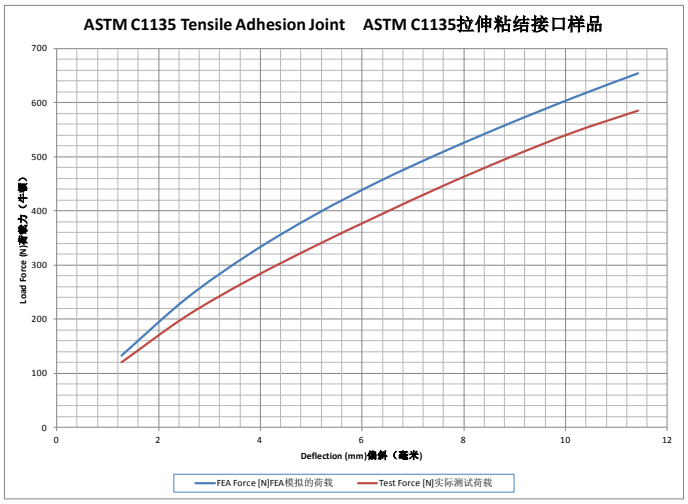

Figure 1. Induced load versus sample deflection in ASTM C1135 Tension Tests (typical of 12.7mm x 12.7mm x 50.8mm joint size)
图1. ASTM C1135拉伸试验中的感应载荷与样品偏移（12.7mm x 12.7mm x 50.8mm的典型连接尺寸）

983 Structural Glazing Sealant material. The Axel data models for tension, shear, and biaxial data were then curve-fitted with several material models within the software analysis to find a curve fit which minimized the scaled residuals resulting from the data provided. An incompressible two-parameter Mooney-Rivlin curve fit was selected because it produced minimal scaled residuals. Independent literature indicates that the Mooney-Rivlin material model can accurately represent a material's response up to 100% strain.

The Mooney-Rivlin two parameter model was tested against the results of ASTM C1135 tensile adhesion joint samples by Dow Corning to validate the generate model using a 1.27 mm mesh size. Below documents the model used to replicate the ASTM C1135 test sample where the size of the silicone joint was 50.8 mm x 12.7 mm x 12.7 mm. For computational efficiency, the size of the glass adhered to the silicone was reduced to the surface area of the silicone sample itself.

Results of the ASTM C1135 test model were compared to the results of physical specimens of the same batch of silicone used in the Axel Products curve-fitted data. Figure 1 documents the load vs. deflection diagrams of the ASTM C1135 test results and the C1135 ANSYS FEA results. Additionally, results at each 1.27 mm of deflection are provided in Table 1, along with the resultant force error at each point.

The results within the curve-fitting regime in a single silicone batch indicated a maximum recorded error of 17.6% in the range of 3.81 mm deflection, or approximately 30% nominal strain. In all cases, the FEA results over-predicted the physical test results. Observation of the percent error within the silicone batch indicated that while the material properties appeared stiffer than the material tested, the offset between the tested and modeled materials is consistently between 11% and 18% through the modeled extensions. It should be noted that the strain rate of the data used to generate the FEA material properties and the data used to generate the ASTM C1135 test results were different; the FEA material properties were generated at 0.01 s^{-1} strain rate, while the ASTM C1135 test results were generated at 0.0167 s^{-1} strain rate. It is known that rate of strain of hyperelastic materials affects the modulus properties; the effects of the rate of strain were not explicitly analyzed in this paper [Yarosh et.al].

FEA results were compared across several batches of silicone in addition to the single batch above (Table 2). Dow Corning provided three randomly selected data sets from individual batches for error analysis. Results of the sensitivity study indicate the error between the

Deflection [mm] 偏斜	FEA Force [N] 模拟的荷载	Test Force [N] 实际测试荷载	Percent Error (%) 误差率
1.27	133	120	11.2
2.54	238	205	15.7
3.81	322	274	17.6
5.08	393	335	17.4
6.35	455	392	16
7.62	510	447	14.3
8.89	561	498	12.8
10.16	609	545	11.7
11.43	654	585	11.9

Table 1. Estimated error between load determined in the FEA Model and actual load test from specimen prepared with silicone batch used in FEA data model.
表1. 在FEA模型中确定的载荷与采用FEA数据模型中所用硅酮胶批次制备的试验样本进行的实际载荷试验之间的估算误差

Strain (%) 伸长量	Force (N) 荷载				Percent Error 误差率		
	FEA FEA模拟荷载	Batch 1 批次1	Batch 2 批次2	Batch 3 批次3	Batch 1 批次 1	Batch 2 批次2	Batch 3 批次3
25	133	173	200	162	-22.9	-33.3	-17.6
50	290	352	347	282	-17.7	-16.4	2.7
75	455	573	533	429	-20.6	-14.6	6.1

Table 2. Estimated error between loads determined in ASTM C1135 modeled in FEA and actual results of three historical batches of ASTM C1135 testing.
表2. 在FEA中通过ASTM C1135模型确定的载荷与三个ASTM C1135不同批次试验实际结果之间的估算误差

性能有影响，但本文没有详细分析应变率的影响[Yarosh等]。

除了上述单批次之外，还对几个硅酮胶批次的FEA结果进行了比较（表2）。道康宁提供三套由各批次随机选择的数据集用于误差分析。灵敏度研究结果显示，FEA硅酮胶模型与样品批次之间的最大报告误差值在25%的应变下为33.3%。与批内比较不同，批间比较显示FEA模型过低预测了物理试验中的感应载荷。由批间比较计算出的误差缺乏批内研究中两种材料之间的一致偏移。同样，应当注意历史数据的应变率产生时的载荷率与FEA模型的应变率不同。历史数据生成时的载荷率为50.8 mm / min，等于0.067 s^{-1}的应变率。

图2和图3中的应力分布图显示了FEA模型在0.76mm偏移和1.78 mm偏移下的结果。在这些偏移条件下，感应力分别为84.1 N和177.9 N，大约相当于硅酮结构胶通常考虑的限制应力的100%和200%。

注意，在这两种情况下，沿着周长计算的应力峰值，且硅酮胶样品中的应力是非常不均匀的。硅酮胶与相邻基层之间的高差刚度导致应力不均匀分布。以上显示的结果与ASTM C1135试验中所观察到的典型失效传播从测试样本的周边开始是一致的。

在新提出的硅酮密封胶连接背后的基本原理可参考ASTM C1135试验样品的结果。在负荷载下的典型幕墙组件中，在硅酮胶以方形的几何形状粘合的位置，在周边密封上的玻璃有限旋转将会引起在硅酮胶连接边缘处的最大活动。支持新密封胶几何形状设计的概念是它允许额外的活动能力，使得玻璃可以更加自由地旋转，而不是迫使密封胶去抵抗边缘处的玻璃有限旋转（理论上在密封胶内促使力偶矩）。图4以图示的方式展示了两种情况下玻璃相对于硅酮胶接口的预期旋转中心。

在1905 mm x 1524 mm的玻璃模型上对所提出的密封胶连接设计进行试验。玻璃的四分之一包括在模型中，以保证计算效率。生成了两个模型：一个用于所提出的密封胶设计（梯形，长边23.81 mm，梯形短边6.35mm，梯形长边12.7 mm），另一个为

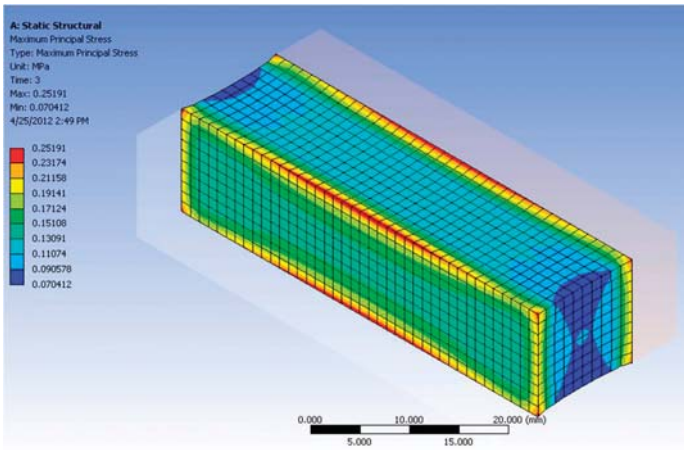

Figure 2. Distribution of Stress at 100% of Allowable Nominal Silicone Stress
图2. 在100%允许公称硅酮胶应力下的应力分布

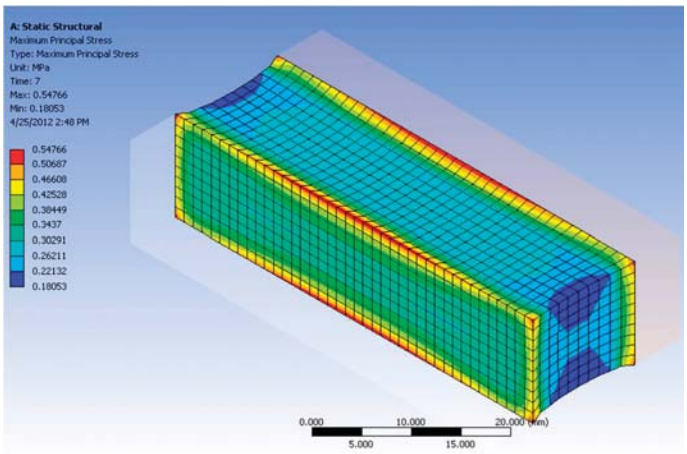

Figure 3. Distribution of Stress at 200% of Allowable Nominal Silicone Stress
图3. 在200%允许公称硅酮胶应力下的应力分布

FEA silicone model and the sample batches has a maximum reported error of 33.3% at 25% strain. Unlike the intra-batch comparison, the inter-batch comparison indicates the FEA model is under predicting the induced loads in the physical tests. The error calculated from the inter-batch comparison lacks the consistent offset between the two materials of the intra-batch study. Again, it should be noted that the strain rate of the historical data was generated at a different load rate than the strain rate of the FEA model. The historical data was generated at a load rate of 50.8 mm / min, equal to a strain rate of 0.067 s^{-1}.

Stress distribution plots in Figures 2 and 3 indicate the results of the FEA models at 0.76 mm deflection and 1.78 mm deflection. At these deflections, the induced forces were 84.1 N and 177.9 N, respectively, which are approximately representative of 100% and 200% of what is typically considered limiting stresses for structural silicones.

Note that in both cases, stress peaks are calculated around the perimeter, and the stress within the silicone sample is highly non-uniform. The high differential stiffness between the silicone and the adjacent substrate causes the stress to be unevenly distributed. The results shown above are consistent with typical failure propagation starting at the perimeter of the testing specimen as observed in ASTM C1135 tests.

The rationale behind the newly proposed silicone sealant joint can be seen in the results of the ASTM C1135 test samples. In a typical curtain wall assembly under negative loads, where the silicone is adhered in a square geometry, the finite rotation of the glass at the perimeter seal will induce the greatest movement at the edge of the silicone joint. The concept behind the new sealant geometry design allows additional movement capacity for the glass to rotate more freely rather than forcing the sealant to fight against the finite rotation of the glass at the perimeter (theoretically inducing a moment couple within the sealant). Figure 4 schematically demonstrates the anticipated center of rotation of the glass relative to the silicone joint in both cases.

The proposed sealant joint design was tested on a 1905 mm x 1524 mm glass model. One quarter of the glass was included in the model for computational efficiency. Two models were generated: one for the proposed sealant design (trapezoid with 23.81 mm long dimension, 6.35mm short trapezoid dimension, and 12.7 mm long trapezoid dimension), and one with a 50.8 mm long rectangular sealant joint, per standard industry practice. The glass was loaded to 9.6 kPa. The results of the models were compared as well as to benchmark stresses in the C1135 model.

The results of the trapezoidal silicone models that indicate maximum

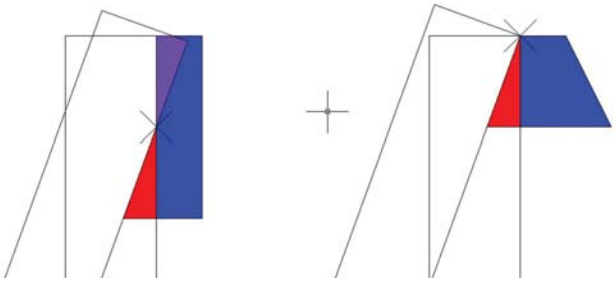

Figure 4. Assumed Glass Rotation for Trapezoidal and Traditional Silicone Joints
图4. 梯形和常规硅酮胶接口的假设玻璃旋转

50.8 mm长矩形密封胶连接，符合标准业界惯例。玻璃被施加荷载至9.6 kPa。模型的结果相互进行比较，并与C1135模型中的基准应力进行比较。

梯形硅酮胶模型的结果显示通过硅酮胶粘合总面积的最大应力不超过0.38 MPa，同时硅酮胶连接边缘上的峰值应力为0.64 MPa。一个类似 ASTM C1135 测试样品的结果带类似边缘应力被加载致 2.29 mm 偏移及 218.6 N 作用力。一个“传统”硅酮胶模型的结果显示硅酮胶粘合总面积不超过0.55 MPa，硅酮胶连接边缘上的峰值应力为0.91 MPa.。一个类似 ASTM C1135 测试样品的结果带类似边缘应力被加载致 3.30 mm 偏移及 293.4 N 作用力。图5至10显示了长、短距在中跨处的应力详情，以及可比较的峰值边缘应力。

前图的结果显示通过在较大的风载下容许硅酮胶随着玻璃旋转可以减小应力。并且，当传统配置中的硅酮胶与C1135样品试验结果进行比较时，硅酮胶连接的设计中所包括的安全系数可能不如所显示的高。

为了确认所提出的硅酮胶接缝不会危及正载荷下的玻璃，将上述硅酮胶连接加至6.2 kPa的正压载荷，以检查硅酮胶连接内的应力分布效应。转角连接应力也与传统硅酮胶连接中的应力相对作出检查，见图11所示。在负风压下，梯形硅酮胶连接的总面积和转角上的应力没有超过传统硅酮胶连接的应力。

测试模型结果

按比例将独特的连接设计增大到真正尺寸的玻璃，采用9.58 kPa（200 psf）的设计荷载，并按照佛罗里达州迈阿密市戴德郡建筑规范的高速飓风区域试验协议进行试验。所遵循的协议是测试应用标准（TAS）TAS 202-94，均匀静态气压试验的程序。该试验方法按照ASTM E330的意向操作，用均匀静态气压差测试外门窗、天窗与幕墙的结构性能。

此测试模型的荷载压力为± 9.58 kPa（200 psf）并进行

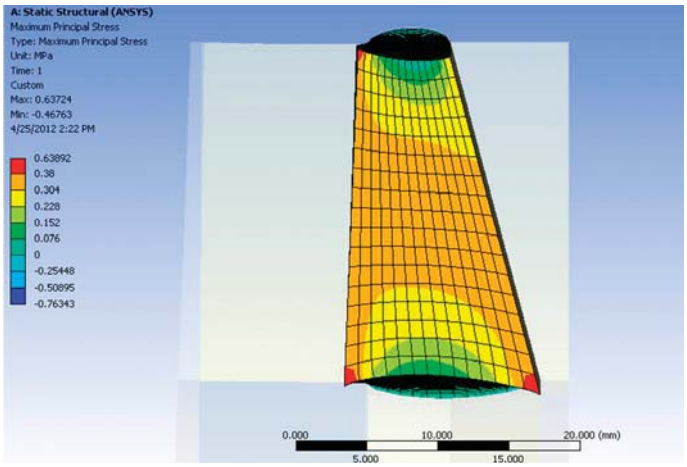

Figure 5. Distribution of Stress at Short Dimension Midspan of Trapezoidal Joint at 23.8 mm orthogonal bond width between glass and sealant
图5. 在梯形接口短尺寸中跨处的应力分布

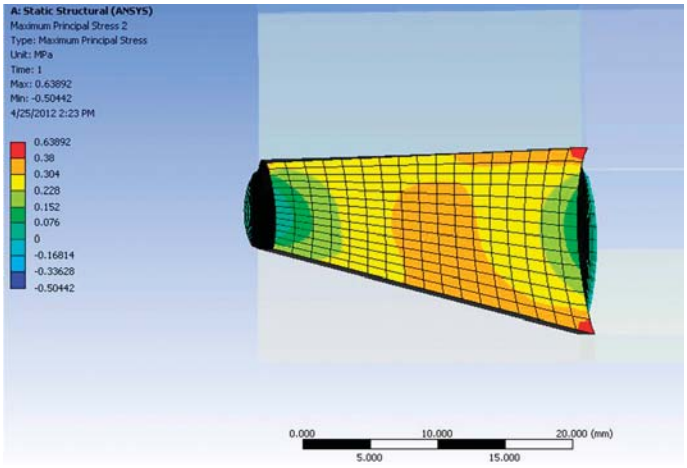

Figure 6. Distribution of Stress at Long Dimension Midspan of Trapezoidal Joint at 23.8 mm orthogonal bond width between glass and sealant
图6. 在梯形接口长尺寸中跨处的应力分布

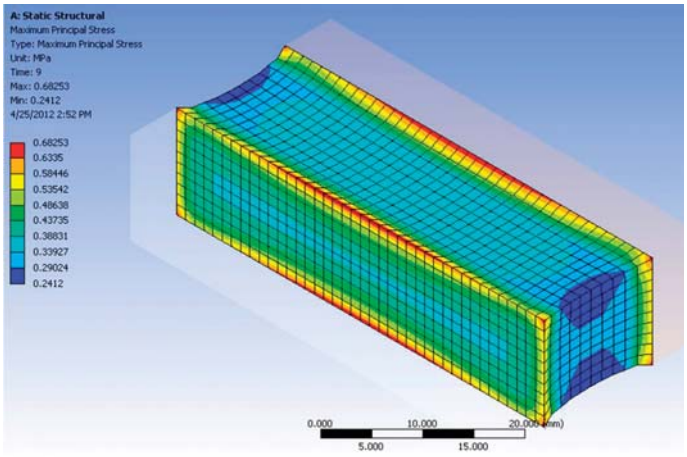

Figure 7. Test Results of ASTM C1135 Tensile Adhesion Joint (typ. 12.7mm x 12.7mm x 50.8mm) with Similar Peak Edge Stresses to Trapezoidal Joint
图7. 在梯形接口上施加类似峰值边缘应力时的ASTM C1135拉伸粘合接口的试验结果（典型尺寸为12.7mm x 12.7mm x 50.8mm）

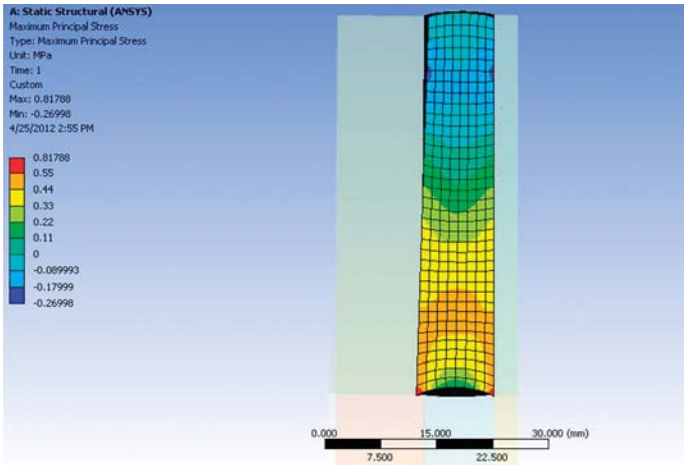

Figure 8. Distribution of Stress at Short Dimension Midspan of Traditional Joint at 50.8 mm bond width
图8. 在常规接口短边中点处的应力分布

stress through the gross area of the silicone bite did not exceed 0.38 MPa, with peak stress along the edge of the silicone joint at 0.64 MPa. The results of a similar ASTM C1135 test sample with similar edge stresses were loaded to 2.29 mm deflection and 218.6 N applied force. The results of a "traditional" silicone model indicate the gross area of the silicone bite did not exceed 0.55 MPa, with peak stress along the edge of the silicone joint at 0.91 MPa. The results of a similar ASTM C1135 test sample with similar edge stresses were loaded to 3.30 mm deflection and 293.4 N applied force. Details of these stresses at the mid-span of both the long and short dimensions, as well as comparable peak edge stresses are shown in Figures 5 to 10.

The results of the preceding figures indicate that a stress reduction can be achieved by allowing the silicone to rotate with the glass under large wind loads. It also shows that safety factors included in the design of silicone joints may not be as high as those indicated when comparing silicone in the traditional configuration to the results of a C1135 sample test.

To confirm that the proposed silicone joint would not compromise the glass under positive loads, the above-mentioned silicone joint was loaded to 6.2 kPa positive pressure to check the effects on the stress distribution within the silicone joint. Corner joint stresses were checked against the stresses in the typical silicone joint; these can be seen in Figure 11. The stresses in both the gross area and the corner of the trapezoidal silicone joint did not exceed those in the traditional silicone joint under negative wind loads.

±14.37（300 psf）试验，以验证TAS 202-94中规定的150%超荷载。测试模型样品制造可适应1524 x 1905mm（60" x 75"）大小的玻璃。试验中使用了两种不同的夹胶膜材料，聚乙烯醇缩丁醛（PVB）和杜邦SentryGlas ®Plus（SGP）；测试模型使用了三种不同类型的单片夹胶玻璃来测试。

- 5mm钢化清玻，2.3mm PVB夹层，5mm钢化清玻（3/16" 钢化清玻，0.090 PVB夹层，3/16" 钢化清玻）
- 5mm钢化清玻，2.3mm SGP夹层，5mm钢化清玻（3/16" 钢化清玻，0.090 SGP夹层，3/16" 钢化清玻）
- 6mm热工强化清玻，2.3mm SGP夹层，6mm热工强化清玻（1/4" 热工强化清玻，0.090 SGP夹层，1/4" 热工强化清玻）

玻璃以23.8mm宽的结构胶以梯形的连接配置直角地投射粘合在阳极氧化铝框架上，如图12中所示。按照传统的计算，结构胶宽度至少需要52.9mm。框架采用标准铝管制成，铝管上采用机械方式附着制动金属块，并有6mm（1/4"）紧固件再每200mm（8"）中心处。1型和2型玻璃严格按照图1所示进行试验。3型玻璃所使用的耐候密封细节上有所变化，不使用泡沫棒，用硅酮结构胶填充矩形空腔。在所有的情况下，硅酮结构胶均不与玻璃边缘处使用的硅酮胶接触。

在测试挠度期间，在实验室中对铝框架和玻璃的中心进行挠度测量。这些挠度在表3-5中报告，并与"指针读数"下表格中注明的位置相对应。表3-5报告呈现有关玻璃单元的空气渗透、水渗

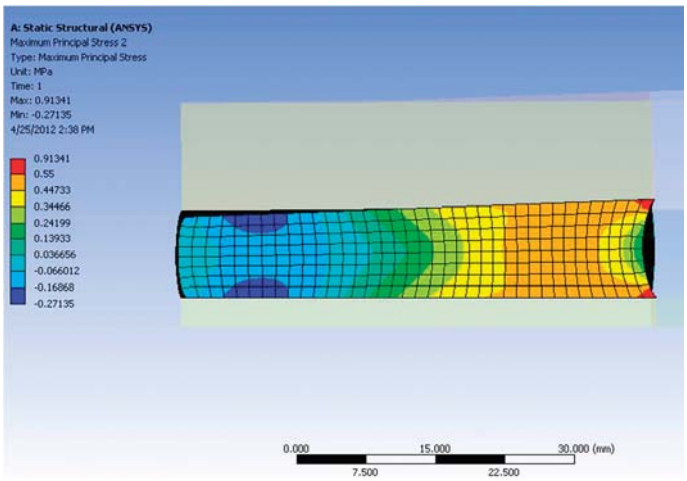

Figure 9. Distribution of Stress at Long Dimension Midspan of Traditional Joint at 50.8 mm bond width
图9. 于50.8 mm黏合宽度，在传统连接长距中跨的应力分布

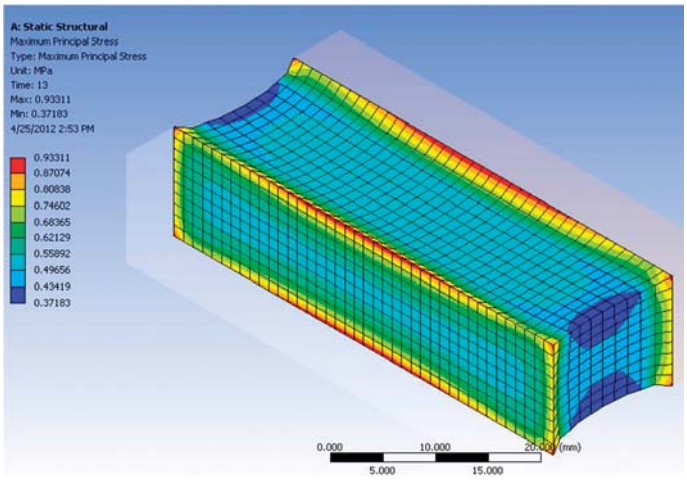

Figure 10. Test Results of ASTM C1135 Tensile Adhesion Joints (12.7mm x 12.7mm x 50.8mm) with Similar Peak Edge Stresses to Traditional Joint
图10. 与常规连接上施加类似峰值边缘应力的ASTM C1135拉伸粘合接口的试验结果（典型尺寸为12.7mm x 12.7mm x 50.8mm）

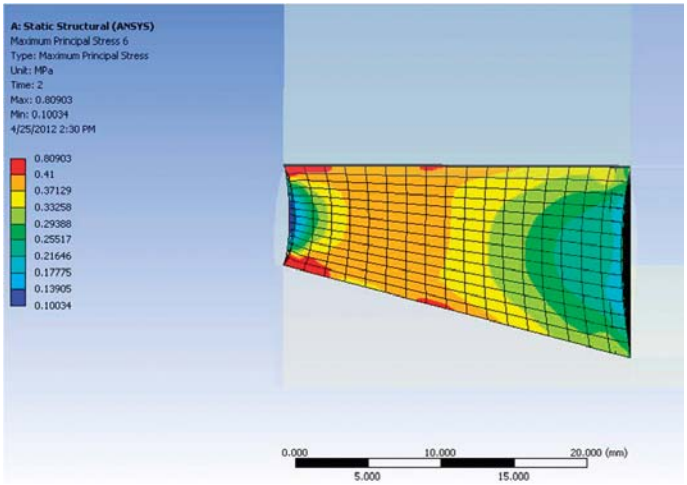

Figure 11. Distribution of Stress at the Corner of the Trapezoidal Silicone Joint under Positive Wind Load (23.8 mm orthogonal bond width)
图11. 在正风压下梯形硅酮胶连接转角的应力分布

Mock-Up Results

The unique joint design was scaled up on a real size piece of glass and a design of 9.58 kPa (200 psf) and tested to the Miami Dade, Florida Building Code's Test Protocol for High-Velocity Hurricane Zones. The protocols that were followed were Testing Application Standard (TAS) TAS 202-94, the procedure for conducting uniform static air pressure test. This test is operated in the spirit of ASTM E330 Standard Test Method for Structural Performance of Exterior Windows, Doors, Skylights and Curtain Walls by Uniform Static Air Pressure Difference.

The loading pressures for this mockup were ± 9.58 kPa (200 psf) with a ±14.37 (300 psf) test to validate 150% overload as specified in the TAS 202-94. The mockup samples were fabricated to accommodate a glass size of 1524 x 1905mm (60" x 75"). Two different laminates were used, Polyvinylbutyral (PVB) and DuPont SentryGlas ® Plus (SGP). Three different monolithic laminated types of glass were used in the mock up testing.

- 5mm clear tempered, 2.3mm PVB interlayer, 5 mm clear tempered (3/16" Clear tempered, 0.090 PVB interlayer, 3/16" Clear tempered)
- 5mm clear tempered, 2.3mm SGP interlayer, 5 mm clear tempered (3/16" Clear tempered, 0.090 SGP interlayer, 3/16" Clear tempered)
- 6mm clear Heat Strengthened, 2.3mm SGP interlayer, 6 mm clear Heat Strengthened (¼" Clear Heat Strengthened, 0.090 SGP interlayer, ¼" Clear Heat Strengthened).

The glass was attached to an anodized aluminum frame as shown in Figure 12 with a 23.8 mm structural bite orthogonally projected through the trapezoidal joint configuration. Conventional calculation would have required a minimum structural bond width of 52,9 mm. The frame was constructed out of a standard aluminum tube to which a brake metal shape was mechanically attached with 6mm (¼") fasteners 200mm (8") on center. Glass type 1 and 2 were tested exactly as shown in Figure 3. The weatherseal detail used with glass type 3 was altered by omitting a backer rod and filling the rectangular cavity with the structural silicone. In all cases the structural silicone was not in contact with the silicone used at the glass edge.

During test deflection, measurements were taken of the aluminum frame and the center of glass at the testing laboratory. These deflections are reported in Tables 3-5 and correspond to the locations noted in the tables under "Indicator Reading." Tables 3-5 report the data

透和静态荷载的数据。

在设计风压± 9.58 kPa（200 psf）且包括± 14.37 kPa（300 psf）的超荷载条件下，三种类型的玻璃类型符合迈阿密市戴德郡规范TAS 202-94的要求。

此测试模型清楚地显示，独特的硅酮胶连接设计通过了±9.58 kPa（200 psf）的风压设计标准，且可以承受± 14.37（300 psf）的超荷载。用于玻璃结构连接的硅酮材料与独特的连接设计相结合，证明了能力其有可能超越目前公认的SSG设计方法。

对出众的结构硅酮胶玻璃装配和结合新设计的结论

如前所述，缺少可信的技术出版物使得新设计方法需要仔细考虑，或者需要提高结构硅酮密封胶的设计强度。以下是所提出的一项建议方法，使用有限元分析的可靠的系统性方法，旨在改进结构粘合配置和超越传统数值的最大应力设计。

- 建立准确的FEA模型
- 从常规公式和设计应力设计，开发一个结构连接的FEA模型
- 开发一种优化的FEA模型用于替代的连接设计和密封胶设计强度
- 将常规连接模型与替代模型进行比较，以确定通过替代设

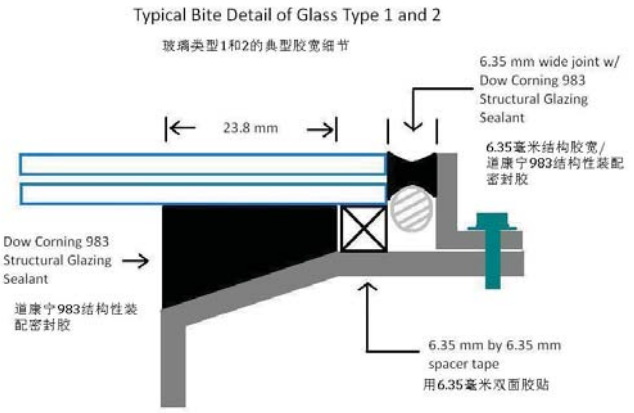

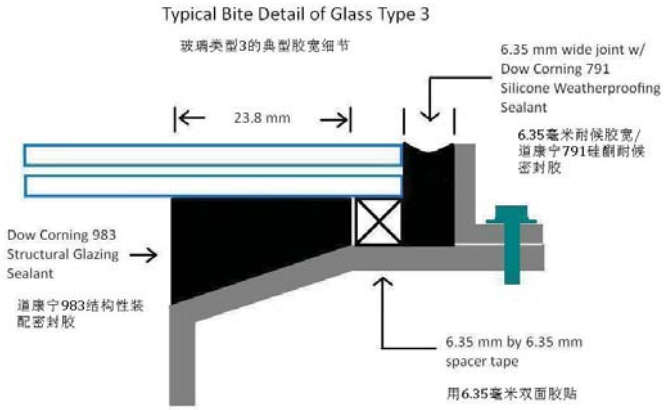

Figure 12. Detail of horizontal and vertical attachment in tested mockups
图12. 试验实体模型中的水平与竖直连接节点图

taken on the air infiltration, water infiltration, and static loading of the glass units.

The three types of glass met the Miami Dade Code requirements for TAS 202-94 at a design wind pressure of ± 9.58 kPa (200 psf) which included a ± 14.37 kPa (300 psf) overload.

This mock up clearly showed that the unique silicone joint design passed the windload design criteria for ±9.58 kPa (200 psf) and survived the ± 14.37 (300 psf) overload. The silicone material used for the structural attachment of the glass in combination with the unique joint design has demonstrated the potential to perform beyond current accepted methods for SSG design.

Conclusions on Superior SSG and incorporating a new design

As mentioned previously, the lack of credible technical publications has created a need to properly consider new design methods or increases to design strength of structural silicone sealant. The following is a proposed method for a credible and systematic approach for use of Finite Element Analysis for advanced design of structural bite configuration and appropriate maximum stresses beyond traditional.

- Establish an accurate FEA model
- Develop an FEA model of a structural joint designed by the conventional formula and design stress
- Develop an optimized FEA model for the alternative joint design and sealant design strength

Figure 13.Picture of actual mock-up assembly used in testing validation
图13. 测试验证中使用的实际模型组件图片

计减小最大应力的分布

- 用实际性能测试模型幕墙单元验证替代连接设计

用复杂的计算软件生成了有限元分析模型，其中需要两个主要的要素。第一个也是首要的要素是适当选择一种可以在期望性能范围内准确预测材料特性的材料模型。第二个要素是一套准确的数据，是通过常规实验方法测试并由模型软件确认的，可以准确预测材料的真实性能。

按照ASTM C1135测试的拉伸粘合连接已经成为一种标准的试验方法，用于理解在幕墙单元中结构硅酮胶玻璃装配连接原型几何形状中的结构密封胶应力/拉紧关系考虑到与拉伸粘合连接的预测材料性能相关的常规结构设计方法的历史已经证明，那么可以确信通过选择预测材料性能的适当模型可以预测拉伸粘合连接的性能。

替代设计过程的下一步是预测常规连接设计在最大载荷下的应力分布。理解设计载荷下的拉伸粘合连接所产生的峰值力是非常重要。

使用FEA模型软件时，下一步将是确定最佳的连接几何形状，以预测在密封胶连接内的总体较低的累积应力分布，从而达到减少铝或金属框架构件有吸引力的条件，同时不牺牲硅酮结构硅酮密封胶能力的损坏载荷。

两种模型的比较对于期望的密封胶性能具有物理学意义，包括实际试验结果、不同连接内生成力的合理期望、不同连接几何形状的适当验证（如按照ASTM C1135测试的拉伸粘合连接）等。

ASTM C1184概括了结构玻璃装配应用中使用的硅酮密封胶所需的性能。重要的是按照ASTM 1135试验方法在不同潜在环境条件下（与温度和环境接触有关）的最小拉伸强度为350 kPa（50 psi）。硅酮密封胶在很广泛的预期温度范围内都具有优良的性能，但在密封胶预期性能方面则存在着一定的差异。

这说明了为替代连接设计选择所使用的密封胶是一项重要的考虑因素。通过ASTM C1135测试仅仅勉强满足ASTM C1184任何要求的结构密封胶不应当考虑为相对于其他选项的首要选择。应当将以较高安全系数符合每一项要求的密封胶作为替代设计和密封胶设计强度的首选。

应使用测试模型来测试以验证对于密封胶的实际性能和有限元模型分析的性能的预测和比较，以确保任何对现有已成功证明40多年标准惯例，具有足够的能力。对一次性事件如炸弹爆炸和冲击应用的性能仍需要适当考虑以相称的建筑法规和业界认可的测试方法来测试实际的模型。

Title of Test 测试项目	Results 结果					
Air Infiltration at 75.2 Pa (1.57 psf ,25 mph) 75.2Pa(1.57psf ,25 mph)的空气渗透率	<0.18m³/m²/hr (<0.01 cfm/ft²)					
Air Infiltration at 300 Pa (6.24 psf, 50 mph) 300Pa(6.24psf ,50 mph)的空气渗透率	<0.18m³/m²/hr (<0.01 cfm/ft²)					
	Indicator Reading (mm) 指针读数					
Structural Loads 结构荷载 50% of Test Pressure 7.19 kPa (+150 psf) 50%的测试正风压7.19KP	#1 Midpoint short span 短边的中点	#2 Top corner 顶部转角	#3 Quarter point long span 长边的1/4点	#4 Mid point long span 长边的中点	#5 Bottom corner 底部转角	#6 Glass Center 玻璃中心
Maximum Deflection 最大挠度	2.8	3	3.8	4.3	3.8	26.9
Permanent Set 永久变形	2.3	2.3	2.3	2.3	2.3	4.1
Design Pressure 9.58 kPa (+200 psf) 设计正风压 9.58KPa						
Maximum Deflection 最大挠度	3.3	3.6	4.8	5.6	4.8	31.8
Permanent Set 永久变形	2.5	2.8	2.8	2.8	2.8	5.3
50% of Test Pressure -7.17 kPa (-150 psf) 50%的测试负风压7.17KPa						
Maximum Deflection 最大挠度	4.3	5.1	5.3	6.1	5.3	34.5
Permanent Set 永久变形	3.3	3.8	3.6	3.8	3.6	6.1
Design Pressure -9.58 kPa (-200 psf) 设计负风压 9.58KPa						
Maximum Deflection 最大挠度	4.8	6.1	6.1	7.9	6.9	39.9
Permanent Set 永久变形	3.6	4.3	3	4.1	3.8	6.1
Water Infiltration 水渗透率 15% Positive Design Pressure 1.44 kPa (+30 psf) 15%的设计正风压144 kPa	No Penetration 无渗透					
Test Pressure 14.37 kPa (+300 psf) 测试正风压 14.37KPa						
Maximum Deflection 最大挠度	7.9	9.4	11.2	12.4	10.9	44.5
Permanent Set 永久变形	5.8	6.9	7.1	7.6	7.4	9.9
Test Pressure -14.37 kPa (-300 psf) 测试负风压 14.37KPa						
Maximum Deflection 最大挠度	3.8	5.6	7.4	8.1	6.9	45.5
Permanent Set 永久变形	0.8	1.3	1	1	0.8	4.6
Forced Entry - ASTM F 588-07 抗外力 ASTM F588-07	Pass 通过					

Table 3. Results for Glass Type 1 tempered clear and PVB interlayer
表3. 玻璃1型钢化清玻和PVB夹层的结果

Title of Test 测试项目	Results 结果					
Air Infiltration at 75.2 Pa (1.57 psf ,25 mph) 在75.2Pa(1.57psf ,25 mph)的空气渗透率	<0.18m3/m²/hr (<0.01 cfm/ft²)					
Air Infiltration at 300 Pa (6.24 psf, 50 mph) 在300Pa(6.24psf ,50 mph)的空气渗透率	<0.18m3/m²/hr (<0.01 cfm/ft²)					
	Indicator Reading (mm) 指针读数					
Structural Loads 结构荷载 50% of Test Pressure 7.19 kPa (+150 psf) 50%的测试正风压7.19KP	#1 Midpoint short span 短边的中点	#2 Top corner 顶部转角	#3 Quarter point long span 长边的1/4点	#4 Mid point long span 长边的中点	#5 Bottom corner 底部转角	#6 Glass Center 玻璃中心
Maximum Deflection 最大挠度	4.6	5.3	6.1	6.6	4.6	21.1
Permanent Set 永久变形	2.8	3.3	3	3.3	2.8	3
Design Pressure 9.58 kPa (+200 psf) 设计正风压 9.58KPa						
Maximum Deflection 最大挠度	5.3	6.1	7.4	8.1	5.6	25.7
Permanent Set 永久变形	3.3	3.8	3.8	3.8	3	3.6
50% of Test Pressure -7.17 kPa (-150 psf) 50%的测试负风压7.17KPa						
Maximum Deflection 最大挠度	2.8	2.5	4.1	4.8	4.6	22.6
Permanent Set 永久变形	1.5	0.8	1.3	1.8	2.5	2.3
Design Pressure -9.58 kPa (-200 psf) 设计负风压 9.58KPa						
Maximum Deflection 最大挠度	3.8	3.8	5.8	6.6	5.8	27.7
Permanent Set 永久变形	1.8	1.5	2	2.3	2.8	3
Water Infiltration 水渗透率 15% Positive Design Pressure 1.44 kPa (+30 psf) 15%的设计正风压144 kPa	No penetration 无渗透					
Test Pressure 14.37 kPa (+300 psf) 测试正风压 14.37KPa						
Maximum Deflection 最大挠度	6.9	8.1	10.2	11.2	7.9	33.3
Permanent Set 永久变形	3.8	4.6	4.3	4.6	3.3	4.1
Test Pressure -14.37 kPa (-300 psf) 测试负风压 14.37KPa						
Maximum Deflection 最大挠度	6.4	7.4	9.7	11.2	8.6	36.6
Permanent Set 永久变形	2.3	2.3	2.8	3	3.6	3.8
Forced Entry - ASTM F 588-07 抗外力 ASTM F588-07	Pass 通过					

Table 4. Results for Glass Type 2 tempered clear and SGP interlayer
表4. 玻璃2型钢化清玻和SGP夹层的结果

- Compare conventional joint models and alternative models to determine that distribution of maximum stress has been reduced via alternative design
- Validate alternative joint design with actual performance mock-up curtain wall units

Finite Element Analysis models are generated by complex computing software that requires two main components. First and foremost is the proper selection of a material model that accurately predicts the behavior of a material over the range of expected performance. Second is an accurate data set that has been tested by conventional test methods recognized by the modeling software to accurately predict real world performance of the material.

Tensile adhesion joints tested to ASTM C1135 have become a standard test method to understand the stress/strain relationship of structural sealants in a prototypical SSG joint geometry in curtain wall units. Given the proven history of the conventional structural design methods with correlation to predicted material performance of a tensile adhesion joint, one should be convinced that the selection of the proper model for predicting material behavior would be predictive of the performance of the tensile adhesion joint.

Next in the process for alternative design would be to predict the distribution of forces in a conventional joint design at maximum loads. Understanding the peak forces generated in a tensile adhesion joint stressed to design load is very important.

Using the FEA modeling software, the next step would be to determine the optimal joint geometry to predict an overall lower cumulative stress distribution within the sealant joint to achieve desirable conditions for reduced aluminum or metal framing members without sacrifice to damaging loads to the structural silicone sealant's capability.

Comparison of both models should make physical sense with respect to the expected performance of the sealant including actual test results, reasonable expectation for forces generated within the different joints, and appropriate validation of the different joint geometries such as the tensile adhesion joints tested according to ASTM C1135.

ASTM C1184 outlines the needed performance of a silicone sealant used in structural glazing applications. Of importance is a minimum tensile property of 350 kPa (50 psi) as tested by ASTM 1135 at different potential environmental conditions related to temperature and environmental exposure. Silicone sealants are well behaved over a wide range of expected temperatures, but potential differences exist within the performance expectations of the sealant.

This illustrates an important consideration in selection of the sealant used for alternative joint design. Structural sealants that marginally meet any requirement of ASTM C1184 via ASTM C1135 testing should not be considered as a primary option relative to other choices. Sealants that meet each requirement with a relatively high safety factor should be the primary choices for alternative design and sealant design strength.

Mock-up testing should be used to enable predictive comparison of the actual sealant behavior and predicted behavior from the FEA model to ensure the competency of any deviation from the convention of our current standard that has proven 40+ years of success. Performance to onetime events such as bomb blasts and impact applications still will need proper consideration from current practices of testing actual mock-ups for appropriate building codes and industry accepted test methodologies.

Title of Test 测试项目	**Results 结果**			
Air Infiltration at 75.2 Pa (1.57 psf ,25 mph) **在75.2Pa(1.57psf ,25 mph)的空气渗透率**	<0.18m3/m²/hr (<0.01 cfm/ft²)			
Air Infiltration at 300 Pa (6.24 psf, 50 mph) **在300Pa(6.24psf ,50 mph)的空气渗透率**	<0.18m3/m²/hr (<0.01 cfm/ft²)			
	Indicator Reading (mm) 指针读数			
Structural Loads **结构荷载** 50% of Test Pressure 7.19 kPa (+150 psf) **50%的测试正风压7.19KP**	#1 Top corner **顶端角部**	#2 Mid point long span **长边的中点**	#3 Bottom corner **底端角部**	#4 Glass Center **玻璃中心**
Maximum Deflection **最大挠度**	6.6	6.6	4.1	16.8
Permanent Set **永久变形**	1	1.3	1.5	1.3
Design Pressure 9.58 kPa (+200 psf) **设计正风压 9.58KPa**				
Maximum Deflection **最大挠度**	7.1	8.1	5.6	21.1
Permanent Set **永久变形**	1	1.5	1.8	1.5
50% of Test Pressure -7.17 kPa (-150 psf) **50%的测试负风压7.17KPa**				
Maximum Deflection **最大挠度**	2.8	5.8	6.4	19.6
Permanent Set **永久变形**	0.5	0.8	0.8	1.3
Design Pressure -9.58 kPa (-200 psf) **设计负风压 9.58KPa**				
Maximum Deflection **最大挠度**	5.6	8.6	8.1	23.1
Permanent Set **永久变形**	1.5	1.5	1.5	1.5
Water Infiltration **水渗透率** 15% Positive Design Pressure 1.44 kPa (+30 psf) **15%的设计正风压 144 kPa**	No penetration **无渗透**			
Test Pressure 14.37 kPa (+300 psf) **测试正风压 14.37KPa**				
Maximum Deflection **最大挠度**	9.1	11.4	8.1	29.2
Permanent Set **永久变形**	1.3	1.5	1.5	2
Test Pressure -14.37 kPa (-300 psf) **测试负风压 14.37KPa**				
Maximum Deflection **最大挠度**	7.6	11.9	10.2	29.7
Permanent Set **永久变形**	1.5	2	1.3	1
Forced Entry - ASTM F 588-07 **抗外力 ASTM F588-07**	Pass **通过**			

Table 5. Results for Glass Type 3 Heat Strengthened clear and SGP interlayer
表5. 玻璃 3 型热工强化清玻和 S G P 夹层的结果

References（参考书目）:

Hilliard, J. R., Parise, C. J., and Peterson, C. O. Jr., 1977 "Structural Sealant Glazing", **Sealant Technology in Glazing Systems**, ASTM STP 638, ASTM International, West Conshohocken, PA, pp. 67-99

Carbary, L. D., 2007 **A Review of the Durability and of Performance Silicone Structural Glazing Systems**, Glass Performance Days 2007, Conference proceedings http://www.glassfiles.com/library/article.php?id=1083&search=carbary&page=1 (viewed April 23, 2012)

Haugsby, M. H., Schoenherr, W. J., Carbary L. D., and Schmidt, C. M., 1989 **"Methods for Calculating Structural Silicone Joint Dimensions,"** Science and Technology of Glazing Systems, ASTM STP1054, C. J. Parise, Ed., American Society for Testing and Materials, Philadelphia, pp. 46-57

Zarghamee, M. S., Schwartz, T. A., and Gladstone, M., 1996 "Seismic Behavior of Structural Silicone Glazing," **Science and Technology of Building Seals, Sealants, Glazing, and Waterproofing**, Sixth Volume, ASTM STP 1286, ASTM, pp. 46–59.

Broker, K.A., Fisher, S., Memari, A.M., 2012 "Seismic Racking Test Evaluation of Silicone Used in a Four-Sided Structural Sealant Glazed Curtain Wall System", **Journal of ASTM International**, Volume 9, Issue 3, March 2012 Paper ID JAI104144, Available online at www.astm.org

Yarosh, K. F., Wolf, A. T., Sitte, S., "Evaluation of Silicone Sealants at High Movement Rates Relevant to Bomb Mitigating Window and Curtainwall Design" 2008, **Journal of ASTM International**, Vol. 6, No. 2, Paper ID JAI101953, Available online at www.astm.org

Travis, H. S. and Carbary, L. D., 1998 "Finite Element Analysis of a Structural Silicone Shear Bead used in Skylight Applications," **Science and Technology of Building Seals, Sealants, Glazing and Waterproofing: Seventh Volume**, ASTM STP 1334, Jerome M. Klosowski, Ed., American Society of Testing and Materials,..,

Hagl, A., **"Durability by Design: New Results on Load Carrying Silicone Bonding".** 2008: Third Symposium on Durability of Building and Construction Sealants and Adhesives, Denver CO, June 25